Acta Crystallographica Section F
Structural Biology and Crystallization Communications
ISSN 1744-3091

Preliminary X-ray crystallographic analysis of the secreted chorismate mutase from *Mycobacterium tuberculosis*: a tricky crystallization problem solved

Ute Krengel,[a,b]* Raja Dey,[a] Severin Sasso,[c] Mats Ökvist,[a,b] Chandra Ramakrishnan[c] and Peter Kast[c]

[a]Department of Chemistry and Bioscience, Chalmers University of Technology, PO Box 462, SE-40530 Göteborg, Sweden, [b]Department of Chemistry, University of Oslo, PO Box 1033, Blindern, N-0315 Oslo, Norway, and [c]Laboratory of Organic Chemistry, ETH Zurich, CH-8093 Zurich, Switzerland

Correspondence e-mail: ute.krengel@kjemi.uio.no

Received 5 December 2005
Accepted 3 April 2006

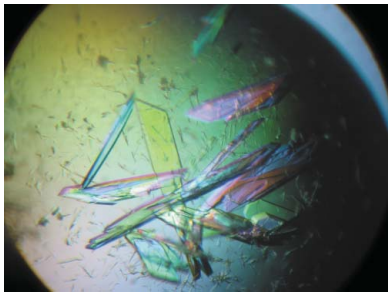

Chorismate mutase catalyzes the conversion of chorismate to prephenate in the biosynthesis of the aromatic amino acids tyrosine and phenylalanine in bacteria, fungi and plants. Here, the crystallization of the unusual secreted chorismate mutase from *Mycobacterium tuberculosis* (encoded by Rv1885c), a 37.2 kDa dimeric protein belonging to the AroQ$_\gamma$ subclass of mutases, is reported. Crystal optimization was non-trivial and is discussed in detail. To obtain crystals of sufficient quality, it was critical to initiate crystallization at higher precipitant concentration and then transfer the drops to lower precipitant concentrations within 5–15 min, in an adaptation of a previously described technique [Saridakis & Chayen (2000), *Protein Sci.* **9**, 755–757]. As a result of the optimization, diffraction improved from 3.5 to 1.3 Å resolution. The crystals belong to space group $P2_1$, with unit-cell parameters $a = 42.6$, $b = 72.6$, $c = 62.0$ Å, $\beta = 104.5^\circ$. The asymmetric unit contains one biological dimer, with 167 amino acids per protomer. A soak with a transition-state analogue is also described.

1. Introduction

The biosynthesis of amino acids is an essential process in living cells as it provides the building blocks for polypeptides and important primary and secondary metabolites. The shikimate pathway is the anabolic pathway employed by bacteria, fungi and plants to synthesize the aromatic amino acids phenylalanine (Phe), tyrosine (Tyr) and tryptophan (Trp) (Haslam, 1993). Chorismate mutase (CM; EC 5.4.99.5) is located at the branch point of the shikimate pathway and channels chorismate into the Tyr/Phe-specific branch. The enzyme catalyzes the conversion of chorismate to prephenate, which is formally a Claisen rearrangement. Chorismate mutases typically accelerate the uncatalyzed rearrangement by roughly one million-fold (Andrews *et al.*, 1973). As one of the few enzymes known to catalyze a pericyclic process, it has generated considerable interest among enzymologists and bioorganic and computational chemists, specifically with respect to the origins of the catalytic efficiency (Andrews *et al.*, 1973; Görisch, 1978; Chook *et al.*, 1994; Haynes *et al.*, 1994; Wiest & Houk, 1995; Lee, Stewart *et al.*, 1995; Kast, Asif-Ullah & Hilvert, 1996; Kast, Asif-Ullah, Jiang *et al.*, 1996; Ma *et al.*, 1998; Mattei *et al.*, 1999; Gustin *et al.*, 1999; Kast *et al.*, 2000; Kienhöfer *et al.*, 2003; Guo *et al.*, 2003; Guimarães *et al.*, 2003; Štrajbl *et al.*, 2003; Zhang *et al.*, 2005).

Structures have been determined for chorismate mutases from *Bacillus subtilis* (Chook *et al.*, 1993, 1994; Ladner *et al.*, 2000), *Escherichia coli* (Lee, Karplus *et al.*, 1995), *Saccharomyces cerevisiae* (Xue *et al.*, 1994; Sträter *et al.*, 1996, 1997) and the catalytic antibody 1F7 with chorismate mutase activity (Haynes *et al.*, 1994). Recently, coordinates have also been deposited in the PDB for chorismate mutases from *Thermus thermophilus* (PDB codes 1ode, 1ufy, 1ui9) and *Clostridium thermocellum* (PDB code 1xho; Xu *et al.*, 2005). Interestingly, these examples comprise three completely unrelated folds: while the structurally characterized enzymes from *B. subtilis*, *T. thermophilus* and *C. thermocellum* have a trimeric pseudo-α/β-barrel fold typical of the so-called AroH class of chorismate mutases (Chook *et al.*, 1994; MacBeath *et al.*, 1998), 1F7 exhibits the characteristic immunoglobulin β-sheet topology. The chorismate mutases of the AroQ class adopt yet another fold, which is dominated by

α-helices. Its prototype, the chorismate mutase domain ($AroQ_p$) of the bifunctional *E. coli* chorismate mutase-prephenate dehydratase (also known as EcCM), is an intertwined homodimer that comprises three α-helices per monomer (Lee, Karplus *et al.*, 1995). This fold has recently been classified as $AroQ_\alpha$ (Ökvist *et al.*, 2006). The allosteric yeast chorismate mutase represents the $AroQ_\beta$ subclass (Ökvist *et al.*, 2006), a more elaborate version of the basic AroQ fold, which shares weak sequence similarity with EcCM and possesses a structurally related active-site domain (Xue *et al.*, 1994; Xue & Lipscomb, 1995; Sträter *et al.*, 1996, 1997).

A third AroQ subclass, initially known as *AroQ (Xia *et al.*, 1993; Calhoun *et al.*, 2001; Sasso *et al.*, 2005) and recently classified as $AroQ_\gamma$ (Ökvist *et al.*, 2006), comprises a group of chorismate mutases that exhibit convincing sequence similarity to other AroQ sequences only in the N-terminal moiety (Sasso *et al.*, 2005; Ökvist *et al.*, 2006). These enzymes are about twice the size of the classical $AroQ_\alpha$ domain and feature a cleavable signal peptide responsible for the export of these chorismate mutases from the cytoplasm (Xia *et al.*, 1993; Calhoun *et al.*, 2001; Sasso *et al.*, 2005). It has been speculated that $AroQ_\gamma$ enzymes may play some role in the pathogenicity of its producer organism (for a discussion and references, see Sasso *et al.*, 2005). Primary structure comparisons suggested that $AroQ_\gamma$ proteins also have other structural peculiarities (MacBeath *et al.*, 1998; Sasso *et al.*, 2005). In particular, a critical amino-terminal segment carrying a conserved active-site arginine is lacking in $AroQ_\gamma$ chorismate mutases. Instead, a homologous helical segment is present in the middle of the polypeptide chain, indicating that the structure of the exported $AroQ_\gamma$ proteins must be topologically distinct from those of the other known AroQ prototypes (Sasso *et al.*, 2005). To investigate this issue and to gain insights into the structure–function relationship of these enzymes, which have the potential to serve as formidable specific drug targets, we have set out to determine the high-resolution crystal structure of the secreted chorismate mutase from the model pathogen *Mycobacterium tuberculosis* (*MtCM; encoded by open reading frame Rv1885c in strain H37Rv), which represents the first characterized example of an $AroQ_\gamma$ fold (Ökvist *et al.*, 2006).

However, crystallization of this enzyme turned out to be non-trivial. While small well ordered crystals could readily be obtained within less than half an hour of setting up the drops, it seemed impossible to obtain (fewer and) larger crystals with better diffraction quality. Common strategies to increase crystal size are to lower the precipitant or protein concentration, thereby moving in the phase diagram from a condition of high supersaturation (where nucleation occurs) to a concentration of lower supersaturation (thus reducing the number of spontaneously formed nuclei, but still staying within the 'labile' zone where nucleation can occur; Mikol & Giegé, 1992). Another well known factor that can influence nucleation is the temperature, which has an impact both on the phase diagram itself and on equilibration kinetics. As an alternative to temperature variation, the equilibration time might be influenced more predictably by applying a layer of oil on top of the reservoir of a vapour-diffusion setup (Chayen, 1997). In this way, equilibration is slowed down, warranting controlled entry into the 'labile' nucleation zone.

All of these protocols work relatively well if the nucleation rate increases gradually upon increasing precipitant or protein concentration. However, if instead there is an abrupt increase in nucleation rate, it can be very difficult to hit the point optimal for both nucleation and crystal growth (if such a point exists at all). In these cases, the application of seeding techniques may be attempted (Stura & Wilson, 1992; Stura, 1999), which approach the problem from the opposite end by placing crystal nuclei in the form of small seeds into the metastable zone optimal for crystal growth. Finding conditions appropriate for seeding has its own inherent difficulties, however, as the metastable zone can be rather narrow and excursions to either side of the phase diagram will inevitably result in either extensive secondary nucleation or dissolution of the seeds. If only little protein is available, this adds to the challenge. A few years ago, two new approaches to the problem were described (Saridakis *et al.*, 1994; Saridakis & Chayen, 2000). The first method involves diluting microbatch drops after incubating them for several hours under spontaneous nucleation conditions (Saridakis *et al.*, 1994), while the second approach relies on transferring cover slips of hanging-drop vapour-diffusion setups from nucleation conditions to the metastable zone (Saridakis & Chayen, 2000). In the present report, we describe the crystal optimization of a protein target that crystallizes very rapidly and show that this problem can be solved by adapting the approach by Saridakis & Chayen (2000) to very short crystallization times.

2. Experimental procedures, results and discussion

2.1. Crystallization

Two different protein batches were used for crystallization. In both cases, recombinant *MtCM was prepared from *E. coli* strain KA29 as described in Sasso *et al.* (2005) and concentrated to 10–20 mg ml^{-1}. Immediately prior to crystallization setups, the protein solutions were centrifuged at 10 000 rev min^{-1} for 10 min at 277 K in order to spin down any floating particles and aggregated insoluble protein. Stan-

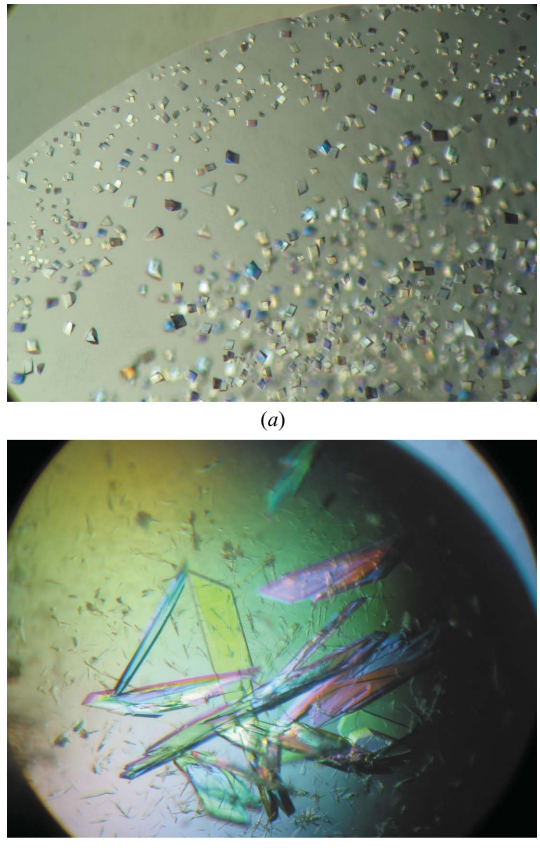

(*a*)

(*b*)

Figure 1
(*a*) Photograph of *MtCM crystals obtained straight from initial screens (crystal size ~20 µm). (*b*) Photograph of *MtCM crystals from optimized crystallization conditions (crystal size ~1 mm in the longest dimension).

dard initial crystallization tests were then performed by the hanging-drop vapour-diffusion method in 24-well tissue-culture plates (Göteborgs Termometerfabrik, Sweden) using siliconized glass cover slips from Hampton Research (CA, USA).

For the first crystallization trials, we used a 175-residue version of *MtCM (encoded on plasmid pKTU3-HCT) devoid of the cleavable signal peptide but containing a C-terminal His tag (Sasso *et al.*, 2005). The protein sample (12.6 mg ml^{-1}) was dissolved in 20 m*M* potassium phosphate buffer pH 7.5. Structure Screen 1 (Molecular Dimensions Ltd, England) gave a few leads, which were optimized, with the best preliminary condition consisting only of 15% PEG 8000 (without buffer). In order to explore different conditions which were not limited by the use of phosphate as buffer, we then switched to protein (18.6 mg ml^{-1}) buffered with 20 m*M* Tris–HCl pH 8.0. This time, the leaderless untagged 167-residue version of *MtCM encoded by plasmid pKTU3-HT was used (Sasso *et al.*, 2005). The first screen at room temperature (293 K) gave a hit for condition No. 18 (0.2 *M* sodium acetate, cacodylate pH 6.5, 30% PEG 8000). A shower of small, well shaped and strongly birefringent single crystals appeared within 20 min of the first crystallization setup (Fig. 1*a*). These crystals diffracted to 3–4 Å resolution. Subsequently, an intense effort was invested into optimizing the crystallization conditions and particularly into slowing down crystallization in order to obtain fewer but larger crystals. However, none of the modifications, such as lowering the protein or precipitant concentration, changing the volume ratios and temperature, using additives or layering the reservoirs with various oils *etc.*, proved successful: we either still obtained a shower of small crystals within 20 min of setting up the drops (using a reservoir concentration of $\geq$20% PEG) or we did not obtain any crystals at all. Even seeding did not help. The final breakthrough came when we recalled a publication by Saridakis & Chayen (2000) in which nucleation was initiated at a high precipitant concentration (which is more likely to produce nucleation centres) followed by transferring the drops before crystals became visible macroscopically to reservoirs with a lower precipitant concentration (which is favourable for crystal growth). In our case, crystallization times were extremely short, so the drops needed to be transferred within less than 20 min. After initial tests showed dramatic improvements upon implementing this strategy, we adopted a more systematic approach and devised a grid screen in which both the incubation period before transfer and the concentration of the final reservoir solution were varied. The best results were obtained when suspending the drops (1.5 µl protein + 1.5 µl reservoir solution) over a starting reservoir (1 ml) containing 20% PEG 4000 (in addition to 0.2 *M* sodium acetate and cacodylate buffer pH 6.5) and then transferring them after 5–15 min to reservoirs containing only 5–15% PEG 4000 (other ingredients constant). In this way, huge crystals ($\sim$1 mm in the longest dimension) appeared overnight which did not look perfect but diffracted to beyond 1.6 Å resolution (Fig. 1*b*). In general, lower reservoir concentrations and shorter incubation times coincided with fewer (and larger) crystals, with the reservoir concentration having the larger impact (particularly for concentrations of <10% PEG).

To our knowledge, this is the first time that the technique of Saridakis & Chayen (2000) has been applied to such short crystallization times. Obviously, in time spans as short as a few minutes, equilibration with the reservoir solution cannot occur. Nevertheless, it turned out to be critical for our experiments to initiate crystallization at a PEG concentration of 20% (before transferring the drop to lower concentrations). The reason for this is presumably a rather steep concentration gradient of PEG in the drop immediately after pipetting the reservoir solution onto the protein droplet. In the mixing zone at the interface between protein and precipitant solution, the PEG concentration will be very close to 20%, enabling the formation of crystal nuclei ('shock' nucleation). The locally high PEG concentration will subsequently decrease by diffusion, establishing conditions favorable for crystal growth, provided that the vapour pressure from the reservoir is sufficiently high to prevent rapid dehydration of the drop, thus avoiding further nucleation.

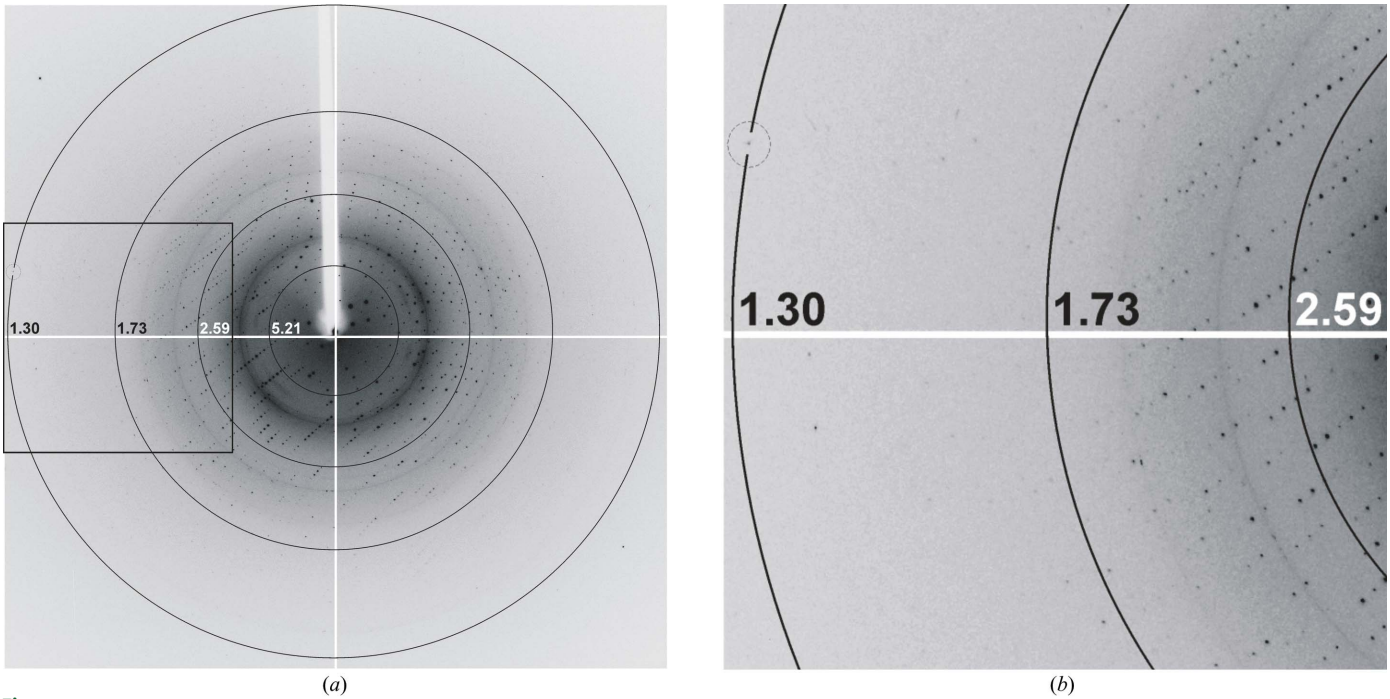

(*a*) (*b*)

Figure 2
Diffraction image from a *MtCM crystal recorded at beamline ID14-4, ESRF, Grenoble. Resolution rings are indicated in (*a*) and a close-up view of the outer rings (*b*) shows that the crystal diffracts to a maximum resolution of 1.3 Å (see encircled reflection in outer resolution ring).

Table 1
Data-collection statistics.

Values in parentheses are for the highest resolution shells included in the final processing.

Data set	Unliganded *MtCM	TSA complex
Synchrotron beamline	ESRF, ID14-4	Max II, I711
Resolution limit† (Å)	31.01–1.55 (1.63–1.55)	38.92–1.64 (1.73–1.64)
Completeness (%)	99.8 (99.8)	99.5 (96.4)
Redundancy	4.1 (4.1)	4.4 (4.0)
Mean $I/\sigma(I)$	10.9 (2.5)	21.4 (7.3)
$R_{\rm merge}$‡ (%)	8.5 (40.0)	5.0 (15.4)
PDB code	2fp1	2fp2

† Crystals diffracted to a maximum resolution of ∼1.3 Å for both data sets (see Fig. 2); however, final data sets only include data to ∼1.6 Å for the following reasons: for unliganded *MtCM, the high-resolution data set was the third of three data sets collected from the same crystal (the preceding two data sets were collected at the MAD peak and edge) and therefore reflections at higher resolution were no longer of acceptable quality and strength. For the TSA complex, data collection was limited to 1.6 Å for technical reasons. ‡ $R_{\rm merge} = \sum |I_i - \langle I \rangle| / \sum I_i$.

2.2. Preparation of a transition-state analogue inhibitor complex

In order to localize and investigate the active site of *MtCM, we performed soaks of the unliganded protein crystals in a solution containing an *endo*-oxabicyclic dicarboxylic acid (referred to here as 'TSA'; Bartlett & Johnson, 1985; Bartlett *et al.*, 1988). This compound is known to be an excellent mimic of the geometry of the transition state of the chorismate mutase reaction and is currently the best inhibitor for a broad range of chorismate mutases (Mandal & Hilvert, 2003), including *MtCM (Sasso *et al.*, 2005). Consequently, it has been used as a ligand in many structural studies of chorismate mutases (Chook *et al.*, 1993, 1994; Haynes *et al.*, 1994; Lee, Karplus *et al.*, 1995; Sträter *et al.*, 1997).

Two different soaking techniques were tested. In order to minimize consumption of the precious compound, we first tried to dissolve a tiny amount of solid TSA directly in a drop containing *MtCM crystals. However, all crystals in the drop dissolved immediately. We then took 0.5 µl of this TSA-containing drop and added it to a 1.5 µl drop containing more *MtCM crystals. After 20 min soaking time, the crystals were cryoprotected by pipetting a drop of mother liquor containing 10% PEG 400 on top of the soak. Thereafter, the crystals were flash-frozen in liquid nitrogen and stored for data collection. Crystal structure analysis (Ökvist *et al.*, 2006) confirmed the presence of TSA in the active site of *MtCM.

2.3. X-ray diffraction analysis

X-ray data were collected and processed as reported by Ökvist *et al.* (2006). *MtCM crystals diffracted to beyond 1.6 Å resolution (diffraction limit 1.3 Å resolution; Fig. 2 and Table 1) and belong to the monoclinic space group $P2_1$, with unit-cell parameters a = 42.6, b = 72.6, c = 62.0 Å, β = 104.5° for the free enzyme and a = 42.9, b = 72.8, c = 61.7 Å, β = 104.0° for the TSA complex. The Matthews parameter $V_{\rm M}$ is 2.9 Å^3 Da^{-1} (Matthews, 1968; calculated for a unit cell containing two protomers per asymmetric unit), which corresponds to a solvent content of 57%. The dimeric nature of *MtCM is consistent with previous biochemical data (Sasso *et al.*, 2005; Prakash *et al.*, 2005). Since sequence alignments (Sasso *et al.*, 2005) suggested homology to the *E. coli* $AroQ_p$ domain, phasing was attempted by molecular replacement using the *E. coli* structure (PDB code 1ecm; Lee, Karplus *et al.*, 1995) as a search model. However, even exhaustive trials did not yield a solution to the problem. A probable reason for the failure is the relatively poor overall sequence homology (16% identity, according to *BLASTP* v.2.2.6 from NCBI; Altschul *et al.*, 1997) between the entire 167-residue *MtCM polypeptide and the structurally characterized 109-residue *E. coli* $AroQ_p$ domain, together with significant structural differences of the C-terminal helices (Ökvist *et al.*, 2006).

We have therefore prepared heavy-atom derivatives (Pb^{II} acetate and Tl^{III} acetate soaks) and solved the structure by the MAD phasing technique based on the Pb^{II} derivative (Ökvist *et al.*, 2006).

3. Concluding remarks

While crystallization of the same protein has been reported very recently by another group (Qamra *et al.*, 2005), our results are distinct since the crystal forms are different (space group $P2_1$ instead of $C2$) and we have significantly higher resolution data (≤1.6 Å *versus* 2.1 Å). Furthermore, we describe the crystallization of free enzyme and a soak with a transition-state analogue, while Qamra and coworkers cocrystallized *MtCM with L-tryptophan.

In addition, this report addresses in detail a general and very challenging crystallization problem and its subsequent solution, which led to the development of an empirical method for crystal optimization for cases with short crystallization times. By applying the optimized protocol, the diffraction limit of the *MtCM crystals could be extended from ∼3.5 to 1.3 Å. This technique, which involves the transfer of crystallization drops to lower concentration reservoirs (varying both reservoir concentration and incubation time before transfer), is particularly useful if the protein of interest crystallizes in a narrow window of conditions and only little protein material is available.

We would like to thank Rosalino Pulido for TSA synthesis and Elin Grahn for help with data collection. At the synchrotron beamlines ID14-4, ESRF, Grenoble and I711, Max II, Lund, we had excellent support from Raimond Ravelli and Yngve Cerenius, respectively. This work has been supported by grants from the Carl Trygger foundation (research grant No. 02:158 to UK and postdoctoral fellowship of RD) from the Glycoconjugates in Biological Systems program of the Swedish National Foundation for Strategic Research (research position of UK), from Novartis Pharma (to SS) and the ETH Zürich (PK).

References

Altschul, S. F., Madden, T. L., Schäffer, A. A., Zhang, J., Zhang, Z., Miller, W. & Lipman, D. J. (1997). *Nucleic Acids Res.* **25**, 3389–3402.
Andrews, P. R., Smith, G. D. & Young, I. G. (1973). *Biochemistry*, **12**, 3492–3498.
Bartlett, P. A. & Johnson, C. R. (1985). *J. Am. Chem. Soc.* **107**, 7792–7793.
Bartlett, P. A., Nakagawa, Y., Johnson, C. R., Reich, S. H. & Luis, A. (1988). *J. Org. Chem.* **53**, 3195–3210.
Calhoun, D. H., Bonner, C. A., Gu, W., Xie, G. & Jensen, R. A. (2001). *Genome Biol.* **2**, 30.01–30.16.
Chayen, N. E. (1997). *J. Appl. Cryst.* **30**, 198–202.
Chook, Y. M., Gray, J. V., Ke, H. & Lipscomb, W. N. (1994). *J. Mol. Biol.* **240**, 476–500.
Chook, Y. M., Ke, H. & Lipscomb, W. N. (1993). *Proc. Natl Acad. Sci. USA*, **90**, 8600–8603.
Görisch, H. (1978). *Biochemistry*, **17**, 3700–3705.
Guimarães, C. R. W., Repasky, M. P., Chandrasekhar, J., Tirado-Rives, J. & Jorgensen, W. L. (2003). *J. Am. Chem. Soc.* **125**, 6892–6899.
Guo, H., Cui, Q., Lipscomb, W. N. & Karplus, M. (2003). *Angew. Chem. Int. Ed. Engl.* **42**, 1508–1511.
Gustin, D. J., Mattei, P., Kast, P., Wiest, O., Lee, L., Cleland, W. W. & Hilvert, D. (1999). *J. Am. Chem. Soc.* **121**, 1756–1757.
Haslam, E. (1993). *Shikimic Acid: Metabolism and Metabolites.* New York: John Wiley & Sons.
Haynes, M. R., Stura, E. A., Hilvert, D. & Wilson, I. A. (1994). *Science*, **263**, 646–652.

Kast, P., Asif-Ullah, M. & Hilvert, D. (1996). *Tetrahedron Lett.* **37**, 2691–2694.
Kast, P., Asif-Ullah, M., Jiang, N. & Hilvert, D. (1996). *Proc. Natl Acad. Sci. USA*, **93**, 5043–5048.
Kast, P., Grisostomi, C., Chen, I. A., Li, S., Krengel, U., Xue, Y. & Hilvert, D. (2000). *J. Biol. Chem.* **275**, 36832–36838.
Kienhöfer, A., Kast, P. & Hilvert, D. (2003). *J. Am. Chem. Soc.* **125**, 3206–3207.
Ladner, J. E., Reddy, P., Davis, A., Tordova, M., Howard, A. J. & Gilliland, G. L. (2000). *Acta Cryst.* D**56**, 673–683.
Lee, A. Y., Karplus, P. A., Ganem, B. & Clardy, J. (1995). *J. Am. Chem. Soc.* **117**, 3627–3628.
Lee, A. Y., Stewart, J. D., Clardy, J. & Ganem, B. (1995). *Chem. Biol.* **2**, 195–203.
Ma, J., Zheng, X., Schnappauf, G., Braus, G., Karplus, M. & Lipscomb, W. N. (1998). *Proc. Natl Acad. Sci. USA*, **95**, 14640–14645.
MacBeath, G., Kast, P. & Hilvert, D. (1998). *Biochemistry*, **37**, 10062–10073.
Mandal, A. & Hilvert, D. (2003). *J. Am. Chem. Soc.* **125**, 5598–5599.
Mattei, P., Kast, P. & Hilvert, D. (1999). *Eur. J. Biochem.* **261**, 25–32.
Matthews, B. W. (1968). *J. Mol. Biol.* **33**, 491–497.
Mikol, V. & Giegé, R. (1992). *Crystallization of Nucleic Acids and Proteins*, edited by A. Ducruix & R. Giegé, pp. 219–239. Oxford University Press.
Ökvist, M., Dey, R., Sasso, S., Grahn, E., Kast, P. & Krengel, U. (2006). *J. Mol. Biol.* **357**, 1483–1499.
Prakash, P., Aruna, B., Sardesai, A. A. & Hasnain, S. E. (2005). *J. Biol. Chem.* **280**, 19641–19648.
Qamra, R., Prakash, P., Aruna, B., Hasnain, S. E. & Mande, S. C. (2005). *Acta Cryst.* F**61**, 473–475.
Saridakis, E. & Chayen, N. E. (2000). *Protein Sci.* **9**, 755–757.
Saridakis, E. E. G., Shaw Stewart, P. D., Lloyd, L. F. & Blow, D. M. (1994). *Acta Cryst.* D**50**, 293–297.
Sasso, S., Ramakrishnan, C., Gamper, M., Hilvert, D. & Kast, P. (2005). *FEBS J.* **272**, 375–389.
Štrajbl, M., Shurki, A., Kato, M. & Warshel, A. (2003). *J. Am. Chem. Soc.* **125**, 10228–10237.
Sträter, N., Håkansson, K., Schnappauf, G., Braus, G. & Lipscomb, W. N. (1996). *Proc. Natl Acad. Sci. USA*, **93**, 3330–3334.
Sträter, N., Schnappauf, G., Braus, G. & Lipscomb, W. N. (1997). *Structure*, **5**, 1437–1452.
Stura, E. A. (1999). *Protein Crystallization: Techniques, Strategies, and Tips*, edited by T. M. Bergfors, pp. 141–153. La Jolla, CA, USA: International University Line.
Stura, E. A. & Wilson, I. A. (1992). *Crystallization of Nucleic Acids and Proteins*, edited by A. Ducruix & R. Giegé, pp. 99–126. Oxford University Press.
Wiest, O. & Houk, K. N. (1995). *J. Am. Chem. Soc.* **117**, 11628–11639.
Xia, T., Song, J., Zhao, G., Aldrich, H. & Jensen, R. A. (1993). *J. Bacteriol.* **175**, 4729–4737.
Xu, H., Yang, C., Chen, L., Kataeva, I. A., Tempel, W., Lee, D., Habel, J. E., Nguyen, D., Pflugrath, J. W., Ferrara, J. D., Arendall, W. B. III, Richardson, J. S., Richardson, D. C., Liu, Z.-J., Newton, M. G., Rose, J. P. & Wang, B.-C. (2005). *Acta Cryst.* D**61**, 960–966.
Xue, Y. & Lipscomb, W. N. (1995). *Proc. Natl Acad. Sci. USA*, **92**, 10595–10598.
Xue, Y., Lipscomb, W. N., Graf, R., Schnappauf, G. & Braus, G. (1994). *Proc. Natl Acad. Sci. USA*, **91**, 10814–10818.
Zhang, X., Zhang, X. & Bruice, T. C. (2005). *Biochemistry*, **44**, 10443–10448.